

## Spontaneous generation of discrete scale invariance in growth models

Y. Huang,<sup>1</sup> G. Ouillon,<sup>2</sup> H. Saleur,<sup>1</sup> and D. Sornette<sup>2,3</sup>

<sup>1</sup>Department of Physics and Astronomy, University of Southern California, Los Angeles, California 90089-0484

<sup>2</sup>Laboratoire de Physique de la Matière Condensée, CNRS URA 190, Université des Sciences, Boîte Postale 70, Parc Valrose, 06108 Nice Cedex 2, France

<sup>3</sup>Institute of Geophysics and Planetary Physics and Department of Earth and Space Sciences, University of California, 3845 Slichter Hall, Box 951567, Los Angeles, California 90095-1567

(Received 15 October 1996)

We suggest that the short-wavelength Mullins-Sekerka instability, together with strong screening effects, generate spontaneously a discrete scale invariance (DSI) in growth processes. A signature of this DSI is the presence of log-periodic oscillations correcting the usual power laws. This is confirmed by extensive numerical simulations on the needle model, using various growth rules (diffusion-limited aggregation, angle screening,  $\eta$  model, and crack approximation) on systems containing up to 5000 needles, and by some experimental data on geological cracks. [S1063-651X(97)04705-3]

PACS number(s): 64.60.Ak, 05.20.-y, 61.43.Hv

### I. INTRODUCTION

In a recent series of papers, there has been growing experimental evidence of log-periodic structures decorating the main power-law behavior in acoustic emissions prior to rupture [1] and in the seismic precursory activity before large earthquakes [2]. Log-periodic oscillations have also been documented in the fractal structure of arrays of cracks in geological media [3]. These log-periodic structures are the expression of *discrete scale invariance* (DSI), the property of a system that is invariant under a *discrete* set of dilatations only. (It is crucial not to confuse DSI with the existence of a discrete scale. For instance, a square lattice is a discrete system, but does not have discrete scale invariance.) Unlike continuous scale invariance, which is very common in all the critical phenomena of nature, DSI was considered, until recently, as the artifact of man-made, discrete fractals or hierarchical constructions. It is not necessarily so, however. Formally, discrete scale invariance corresponds to complex critical exponents, a situation which is actually possible in nonunitary systems like geometrical systems with nonlocal properties (percolation, polymers, and their generalizations), or in system models with disorder (spin-glasses) on *nonfractal* lattices [4]. DSI has also recently been seen quite clearly in the mass-radius scaling relationship of diffusion-limited-aggregation (DLA) clusters [5].

The common aspect of the works [1–3,5] is that they can all be ascribed to growth processes: the question arises of the possible existence of a common origin for DSI in growth dynamics. Indeed, we would like to describe here in some detail a mechanism that seems at work quite generally in *Laplacian* or *diffusive* growth processes. Consider as an archetypal example, a system of parallel identically spaced cracks of the same length growing quasistatically under the action of a destabilizing stress. Excluding the possibility of branching, imagine they grow in size until a state where every other crack stops, and the others begin to grow at a faster rate. Imagine then that the whole process repeats itself, so a succession of period doubling occurs. If each period doubling occurs over a short time compared to the time between them, a set of discrete characteristic crack length

scales are selected, scaling according to a geometrical series. A crack system is thus formed with *discrete scale invariance*, while at the beginning all we had was the existence of a discrete scale (the initial crack spacing). This physical scenario is depicted schematically in Fig. 1. Whether it is possible or not is the subject of this paper. We note that similar ideas have been advanced for thermally induced cracks in brittle solids [6].

We propose that the first ingredient in the cascade of period doubling be the Mullins-Sekerka instability [7], whose underlying mechanism is nothing else but the well-known “lighting rod effect”: in the presence of a Laplacian field (like in electrostatics, DLA growth processes, and in tensorial version in elasticity), the gradient of the field concentrates on domains having a large curvature, therefore leading to their enhanced instability. As a result, the Mullins-Sekerka instability is a short-wavelength (“ultraviolet”) instability and the smallest wavelength allowed is always the most unstable (that there is such a smallest wavelength follows from the initial discrete scale). To have a whole cascade however, it is necessary that the crack growth keeps on showing a sequence of period-doubling instabilities all along the growth process. This, of course, is not obvious: even if the shortest

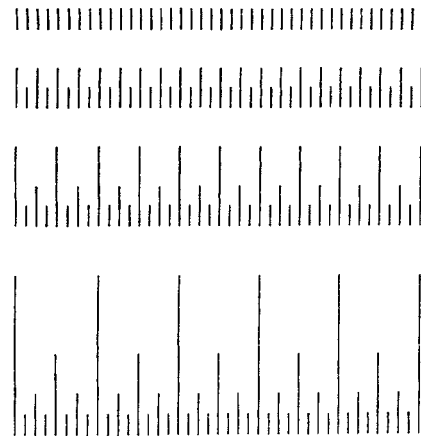


FIG. 1. Schematic drawing of the period-doubling cascade of the growth of a system of parallel cracks or needles.

wavelength is the most unstable, all the other longer wavelengths are also unstable and should grow all together, mixing up the subtle period doubling. We suggest in this paper that *nonlinear* interactions between the unstable modes lead to a succession of period doubling due to screening, the next subharmonic catching up and eventually screening the leading unstable mode. We thus have a sequence of dynamical phases in each of which a single mode dominates. After a while, this mode becomes itself effectively unstable and the mode of twice its period becomes the next dominating mode, and so on. This picture must be taken with some *caution*: there are big fluctuations that “*blur*” the sequence, and it might not be so obvious either by looking at the time evolution of the cracks, or their spatial arrangement: this will depend on the sample. A more robust criteria for DSI will be the presence of log-periodic fluctuations decorating the main power law.

We base our conclusions on four different sets of evidence.

(i) We first present a simple perturbative analysis of the leading nonlinear interaction between two unstable modes. It shows that, if in the linear regime all wavelengths are unstable, the nonlinear interaction leads, by a screening mechanism, to a slowing down of the growth of the most unstable one by the presence of its subharmonic. This is the precursor of the expected crossover to the phase where the subharmonic catches up, becomes the dominant mode, and screens the previously most unstable mode.

(ii) We then use the hodograph method [8] to tackle the nonperturbative multimode problem and present further evidence of the nonlinear interaction between modes leading to a sequence where the faster growing mode is found to be given by the successive harmonics.

(iii) We then present numerical simulations for the needle problem [9,10] using various growth rules (DLA rule, angle screening rule, and  $\eta$  model) on systems containing up to 5000 needles. We analyze the density of needles as a function of the distance to the base and document clear evidence of log-periodic modulations of the leading algebraic decay.

(iv) Motivated by observations in geological settings on joints [3], we then present numerical simulations of quasi-static crack growth. When taking into account all interactions between cracks, we find a similar behavior as for the needles, namely, log-periodic modulations decorating the average algebraic decay of the crack density. We also present a comparison with geological data on joints exhibiting approximately the period-doubling cascade.

These results are analyzed in detail, with a special emphasis on the possible traps in the statistical analysis of such elusive problems where the *signal-to-noise ratio* is not large. We thus develop synthetic tests, used as null hypothesis, to compare with our results. Taken together with the other previously reported evidences, the result provided by our present analysis suggests a very coherent picture, namely, that *complex* critical exponents are a general phenomenon in rupture and growth phenomena. The needle problem analyzed here is a simplification of general growth processes in that branching is neglected. However, we do not expect this additional feature to modify our main conclusions: branching might make more fuzzy the log-periodic structures by adding more noise on the system. However, the numerical evidence

in this case is still quite clear [5]. In addition to being a reasonable approximation, needles are actually real physical objects, in the form of cracks. Therefore, the problem addressed in this paper is of direct application to rupture phenomena, dealing with objects like cracks, joints, faults, and earthquakes. The present work provides an explanation of the value, often found close to 2 for the preferred discrete scaling ratio, as resulting from the period-doubling cascade of successive Mullins-Sekerka instabilities.

In addition to acoustic emission and seismic foreshocks, DLA, and joints, the physical situation studied here should have immediate applications to the flanks of oceanic ridges, to the cracking of mud in deserts and dried up lakes, to crevasses in glaciers, and to thermally induced cracks in geothermal energy exploitation, as pointed out in [6]. We also expect it to apply to more general situations in the presence of additional long-range interactions, as in the side branching of parallel stripe ferrofluids [11] in which the Laplace equation stems from the fluid incompressibility and the additional long-range force is due to magnetic interactions. It would also be worthwhile exploring the possible application of our ideas to the various systems falling in the DLA class or related to it, such as electrodeposition, dendritic crystal growth, and viscous fingering. All are variations of the problem of the time development of a domain which at each point of its boundary, moves with velocity that is the gradient of its Green’s function. In this situation, instabilities of the Mullins-Sekerka type can occur and it is an intriguing question as to whether the nonlinear interactions can stabilize the discrete period-doubling cascade found here. In particular, we should mention that recent experiments have observed a spatial period-doubling instability for a regularly spaced array of dendritic tips with period  $a$  in directional solidification [12], when decreasing the growth rate below a threshold [13]. In [13], the critical velocity at which the period doubling occurs is predicted to be a decreasing function of the dendritic spacing. We would thus expect that a succession of period doubling should occur as the dendritic growth rate is further reduced. For a small growth rate, a lot of modes should be unstable simultaneously as in the needle problem we consider here and it is an interesting possibility whether our proposed scenario for the needles could come into play for the dendrites. One should, however, be cautious because the condition for the validity of these calculations for dendrites [13] may fail at small growth rates, for which further complication may occur. Indeed, the diffusion of solute particles acts as a stabilizing factor introducing a characteristic diffusion length, which is inversely proportional to the growth rate. The period-doubling scenario for dendrites holds when the distance between the dendrites is larger than the diffusion length. If the critical velocity decays slower than  $1/a$ , the diffusion length becomes smaller and smaller than the dendrite spacing and the period-doubling cascade should, in principle, continue. In the reverse case, the diffusion of solute particles will modify the physical scenario beyond the point where it becomes larger than the dendrite spacing. We leave for the future the exploration of the cascade of period doubling to the problem of an array of dendrites.

Section II presents our analytical calculations. Section III contains the numerical simulations of needle systems. Sec-

tion IV presents a numerical simulation of an approximate algorithm for crack growth and the comparison with real geological data on joints. Section V contains our conclusions. The Appendix presents an analysis of the null hypothesis according to which the numerical evidence could be the result of chance alone. Our Bayesian's analysis shows that the statistical significance of the conclusion that the log-periodic structure is a genuine physical phenomenon is extremely high.

## II. DISCRETE SCALE INVARIANCE IN LAPLACIAN GROWTH MODELS: SOME ANALYTICAL REMARKS

The first model we discuss is a needle model of Laplacian growth [9,10]. It consists of  $N$  parallel, equally spaced, needles which grow in the same direction, without branching (we chose the needle spacing as the unit of distance). Let us call  $\phi$  the field that determines the growth of the needles. The dynamics is determined by solving Laplace's equation

$$\Delta \phi = 0, \quad (2.1)$$

subject to the constraint that  $\phi$  vanishes on the needles, and that  $\phi$  increases linearly  $\phi \approx Ay$  at large distance from the needles. These boundary conditions together with Eq. (2.1) determine completely the field  $\phi$  for a given needles configuration. The evolution rule of the model is then given by specifying the growth velocity of every needle according to

$$\frac{dl_i}{dt} \equiv E_i \propto \lim_{r \rightarrow 0} \sqrt{r} |\nabla \phi(r + r_i)|, \quad (2.2)$$

where  $r_i$  is the position of the  $i$ th needle tip. Equation (2.2) expresses that the growth velocity is proportional to the total flux of incoming particles (in the language of DLA) or to the stress intensity factor in the language of crack mechanics (the model corresponds exactly to the antiplane crack problem).

### A. Exponential screening

This system is very well known [10], but we wish to remind the reader of a few results that are relevant for what follows. Let us call  $z$  the plane of the needles, with  $x$  along the needles basis and  $y$  parallel to the needles. The problem can be mapped onto a similar problem of needles growing in a star pattern in the  $w$  plane (Fig. 2) through the mapping

$$w = \exp\left(-\frac{2i\pi}{N} z\right). \quad (2.3)$$

Needles in the  $w$  plane now point at angles differing by  $2\pi/N$  and their length is  $l'_j = \exp(2\pi j/N)$ , as can be seen by inserting  $z_n = j + il_j$  in Eq. (2.3). By observing that  $\partial_w \phi = [1/w'(z)] \partial_z \phi$ , a realization of needle dynamics in the  $z$  plane maps onto a realization of the dynamics in the  $w$  plane.

The feature we want to illustrate here is *screening*. To do so, consider now a case with needles of alternate lengths;  $l_{2i+1} = L_1$  and  $l_{2i} = L_0$ . By one more conformal mapping, we can map the exterior of the unit disk in a third complex plane, call it the  $\zeta$  plane, onto the exterior of the star-shaped object formed by the  $N$  needles in the  $w$  plane through [14]

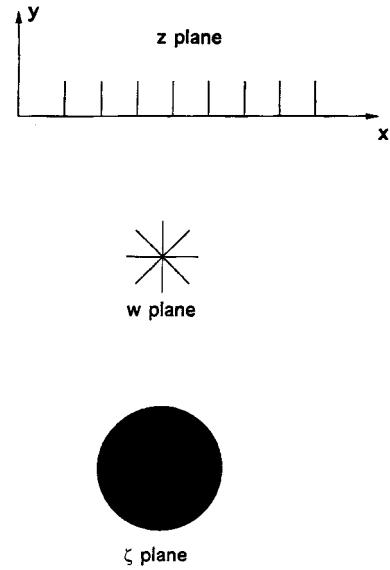


FIG. 2. The conformal mappings involved in solving the dynamics of parallel needles.

$$w = f(\zeta) = C \left( \frac{\zeta^{N/2} + \zeta^{-N/2}}{2} + a \right)^{2/N}, \quad (2.4)$$

where  $a$  and  $C$  are real constants,  $|a| < 1$ . In this mapping, the unit circle of the  $\zeta$  plane maps onto the needles of the  $w$  plane. The solution of Laplace's equation with a field vanishing on the needles in the  $w$  or  $z$  plane follows then from the basic, obvious solution  $\phi = (AN/2\pi) \ln|\zeta|$  in the  $\zeta$  plane. The tip positions maximize  $w$  for  $\zeta$  on the unit circle. The values of the two needle lengths in the  $w$  plane follow

$$L'_1 = C(1+a)^{2/N}, \quad L'_0 = C(1-a)^{2/N}, \quad (2.5)$$

and thus in the  $z$  plane

$$L_1 = \frac{N}{2\pi} \ln C + \frac{1}{\pi} \ln(1+a), \quad L_0 = \frac{N}{2\pi} \ln C + \frac{1}{\pi} \ln(1-a). \quad (2.6)$$

From Eq. (2.2) and with Eq. (2.4), the fields at the two tips in the  $w$  plane are proportional to  $[d^2 f(\zeta)/d\zeta^2]^{-1/2}$  [10], yielding

$$E'_1 \propto (1+a)^{1/2-1/N}, \quad E'_0 \propto (1-a)^{1/2-1/N}, \quad (2.7)$$

with a ratio

$$\frac{E'_0}{E'_1} = \left( \frac{L'_0}{L'_1} \right)^{(N-2)/4}. \quad (2.8)$$

Getting back to the original  $z$  plane, we get the screening for our problem of parallel needles [15]:

$$\frac{E_0}{E_1} = \left( \frac{L'_0}{L'_1} \right)^{(N-6)/4} = \exp\left[ \left( \frac{\pi}{2} - \frac{3\pi}{N} \right) (L_0 - L_1) \right]. \quad (2.9)$$

For  $N$  large, the second term in the exponential is negligible. Setting  $L_1 - L_0 \equiv \Delta > 0$ , the difference in height, we have

$$\frac{E_0}{E_1} \approx \exp\left(-\frac{\pi}{2} \Delta\right), \quad (2.10)$$

establishing that the screening is *exponential*. This is the first ingredient in the problem: height differences lead to a very strong screening and needles of smaller size are very quickly left behind.

### B. The Mullins-Sekerka instability and possible DSI scenario

The second key ingredient concerns instabilities. To handle these, let us replace the needles by a continuous array. Results obtained by keeping a discrete array would be more complicated but contain the same physics. We describe the interface by its coordinate  $y_{\text{int}}(x, t)$  subject to the evolution equations

$$\begin{aligned} \Delta \phi &= 0, \\ v &= \nabla \phi. \end{aligned} \quad (2.11)$$

Again, the boundary conditions are  $\phi=0$  on the interface, and  $\phi \approx Ay$  at large distance from the interface. The Mullins-Sekerka [7] instability corresponds to the fact that perturbations with higher spatial frequencies are more unstable: a perturbation of the interface of the form

$$y_{\text{int}}(x, t) = y_0(t) + \delta(t) \sin kx, \quad (2.12)$$

grows, indeed, like [14]

$$\frac{d\delta}{dt} = Ak\delta. \quad (2.13)$$

For a continuous interface, our model with no short distance cutoff would allow arbitrarily large  $k$ 's. In practice, this does not occur, either because there is actually a surface tension that we neglected so far, or because there is another natural short distance cutoff, e.g., the needle spacing in the problem we discussed first. Let us reinstall this distance  $d$ . This distance defines a Brillouin zone, and associated with it is a maximum meaningful wave vector  $k = \pi/d$ . One is tempted to conjecture that, in the discrete needles problem, the Mullins-Sekerka instability actually gives rise to a sort of *cascade*. Indeed, an extra simplified picture of the interface growth would be that, under random perturbation, the most unstable mode (the one with highest spatial frequency,  $k = \pi/d$ ) grows first: this corresponds to every other needle becoming a bit longer. Following then the discussion in the first part of this section, a strong screening takes place. Assume that the shortest needles are screened so much that they actually stop growing and do not influence further growth of the longest ones. Then we are back to the original situation but with a needle spacing twice as big  $d \rightarrow 2d$ . One then expects that the new most unstable mode, now with  $k \rightarrow k/2$  starts growing, bringing us back to the previous situation with, however, a *rescaling* by a factor  $\lambda = 2$ . This rescaling corresponds so far to properties along the  $x$  axis, i.e., parallel to the needles basis. However, from the equations of motion, it is easy to see that this rescaling should also be observed in the  $y$  direction. Indeed, Eq. (2.13) shows that  $k \rightarrow k/2$  leaves the equation invariant for  $t \rightarrow 2t$ , which in turn, from the

front velocity  $v = \nabla \phi$ , leads to  $y \rightarrow 2y$ . In this caricature, one would imagine that the needles evolution therefore looks something like Fig. 1. Such a pattern obeys *discrete scale invariance*. Let us stress that, in this schematic reasoning, the presence of a short distance (ultraviolet cutoff) is crucial to impose the existence of a highest spatial frequency mode.

This argumentation has weak points, the main one being that events do not happen sequentially. Rather, under a random perturbation, all modes start growing and interfere, with each other, spoiling to some extent the foregoing picture. To what extent exactly do they spoil it?

### C. Two mode nonlinear coupling

While it is very difficult to answer this question rigorously, we can at least provide some interesting arguments. Since in the naive discussion, we were led to consider modes  $k$  and  $k/2$  growing successively, let us now study a perturbation with both of these modes in competition. For notational convenience we set  $k = 2a$ . A perturbation of the interface then looks like

$$y_{\text{int}}(x, t) = y_0(t) + \epsilon(t) \sin ax + \mu(t) \cos 2ax. \quad (2.14)$$

We assume that initially  $\epsilon \ll \mu$  such that the subharmonic is initially of very small amplitude and provides a perturbation on the growth of the main mode. We also take both parameters much smaller than 1. We write similarly the solution of Laplace's equation as

$$\begin{aligned} \phi &= A[y - y_0(t)] + \eta(t) \sin(ax) e^{-a(y-y_0)} \\ &+ \rho(t) \cos(2ax) e^{-2a(y-y_0)} + c(t). \end{aligned} \quad (2.15)$$

It is easy to check that  $\eta = O(\epsilon)$ ,  $\rho = O(\mu)$ . We will keep terms of order  $\epsilon$ ,  $\epsilon^2$ ,  $\mu$ ,  $\mu^2$ , and  $\epsilon\mu$ . The expansion of exponentials generates higher harmonics; what we will do for the moment is simply neglect those larger than  $2a$ , i.e., project onto the two modes we started with. The expression (2.15) solves automatically the Laplace equation. Writing that Eq. (2.15) satisfies the boundary condition  $\phi(y_{\text{int}}(x, t)) = 0$  allows us to get  $\eta$  and  $\rho$  as a function of  $\epsilon$  and  $\mu$ . Computing the gradient of  $\phi$  at the interface and using it to get the interface velocity ( $v = \nabla \phi$ ) and identifying its  $y$  component  $\partial \phi / \partial y|_{y_{\text{int}}}$  with  $dy_{\text{int}}/dt$  gives the equation of evolution of the amplitudes  $\epsilon$  and  $\mu$  of the perturbations

$$\frac{d\epsilon}{dt} = Aa\epsilon + Aa^2\epsilon\mu, \quad (2.16)$$

$$\frac{d\mu}{dt} = 2Aa\mu - A \frac{a^2\epsilon^2}{2}.$$

The first term in each of these equations is the standard Mullins-Sekerka instability. From it we see that the highest (spatial) frequency mode (here  $\mu$ ) grows faster in agreement with Eq. (2.13). What we see also, however, is that the growth of  $\epsilon$  slows down the growth of  $\mu$ . Hence for an initial fluctuation with  $\epsilon \ll \mu$ ,  $\epsilon$  might overgrow  $\mu$  in the long run. In other words, while the perturbation at wave vector  $k$  is the most unstable, it is indeed replaced by  $k/2$  in the long run, like in the naive discussion. Of course, this works only

within the approximation (2.16), that is, only for  $\epsilon$  at most of the order of  $\mu$  and both much smaller than 1, so this is not enough to conclude.

#### D. Use of the complex hodograph method

To go beyond this perturbative analysis, we now use the complex hodograph method [8]. Associated with the foregoing field  $\phi$  we introduce the analytic function

$$\Phi(z) = \phi(x, y) + i\psi(x, y), \quad (2.17)$$

where analyticity requires  $\partial_x \phi = -\partial_y \psi$ ,  $\partial_y \phi = \partial_x \psi$ . Briefly, the hodograph method consists in looking for the solution of the Laplace equation in terms of  $x, y$  as a function of  $\phi$  and  $\psi$ . Introduce the width of the system  $W$ , such that the interface is defined for  $x \in [-W/2, W/2]$  (in the discrete model,  $W=N$  in units where the needle spacing is 1). Then, it is possible to parametrize the complex coordinates of the interface by

$$z_{\text{int}}(s, t), \quad s \in [-AW/2, AW/2], \quad (2.18)$$

with the conditions that  $\partial_s z_{\text{int}}(s, t)$  is analytic and nonzero within the strip  $[-AW/2, AW/2]$  and that [8]

$$\partial_t z_{\text{int}}(s, t) \partial_s z_{\text{int}}(s, t)^* - \partial_s z_{\text{int}}(s, t) \partial_t z_{\text{int}}(s, t)^* = -2i. \quad (2.19)$$

Expression (2.19) writes the growth condition  $v = \nabla \phi$ . It is now possible to find an exact solution to the equations of motion, with again the velocity of the interface being given by the gradient of the field  $\phi$ . A solution based on two harmonics follows from

$$z_{\text{int}}(s, t) = C_0(t) + i \frac{s}{A} + C_1(t) e^{-isa/A} + C_2(t) e^{-2isa/A}, \quad (2.20)$$

and the equations of motion are

$$\begin{aligned} \dot{C}_0 - aC_1 \dot{C}_1 - 2aC_2 \dot{C}_2 &= A, \\ \dot{C}_1 - aC_1 \dot{C}_2 - a\dot{C}_0 C_1 - 2a\dot{C}_1 C_2 &= 0, \\ \dot{C}_2 - 2a\dot{C}_0 C_2 &= 0. \end{aligned} \quad (2.21)$$

On this solution, it is easy to check numerically that for *any* initial amplitudes  $C_1(t=0)$ ,  $C_2(t=0)$ , it is  $C_1$  that dominates at large times.

Another key weakness of the naive argumentation is that it focuses on the sequence with discrete scaling  $k \rightarrow k/2 \rightarrow k/4$ , etc., neglecting other modes that might well spoil this discrete scaling, like for instance  $3k/4$ . To see whether the discrete sequence  $k/2^{n-1} \rightarrow k/2^n$  is indeed ‘‘insensitive’’ to these other modes, let us consider, setting  $k = 4a$ , a solution of the form

$$z_{\text{int}}(s, t) = C_0(t) + i \frac{s}{A} + \sum_{j=1}^4 C_j(t) e^{-ijsa/A}. \quad (2.22)$$

Equations are much more difficult to solve, and the final behavior has to be studied for initial conditions defined in a

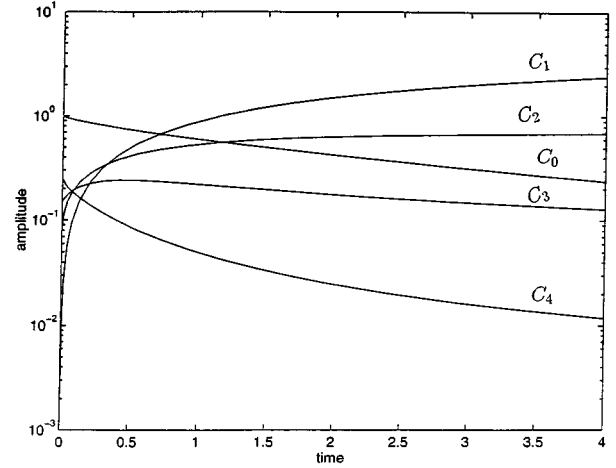


FIG. 3. An example of dynamics for an interface perturbed by four harmonics, as determined using the hodograph method (2.22). The initial values of the amplitudes are  $C_0=1$ ,  $C_1=0.001$ ,  $C_2=0.08$ ,  $C_3=0.15$ , and  $C_4=0.25$ .

four-dimensional space, which is complicated. We have not seen any clear pattern emerging, except that if we start with  $C_1 \ll C_2 \ll C_3 \ll C_4 \ll C_0$ ,  $C_2$  ultimately overgrows  $C_4$ , and then  $C_1$  overgrows  $C_2$ , while  $C_3$  remains almost constant (an example is shown in Fig. 3). Moreover, this behavior extends all the way to the region where  $C_1 \approx C_2 \approx C_3 \approx C_4 \ll C_0$ . This supports the naive picture; however, it is also possible to find rare initial conditions such that ultimately it is  $C_2$ ,  $C_3$ , or  $C_4$  that overgrows the others.

It is not clear to us how to go further. Of course, we are really interested in the limit of an infinity of needles, and therefore a random perturbation would decompose on an infinity of modes. Even if sometimes the sequence  $k \rightarrow k/2$  is spoiled by some special conspiracy of amplitudes, nevertheless in most cases it will occur, so if the perturbation is for some time dominated by a wave vector  $k'$  that does not belong to the initial sequence, this one can nevertheless be the ancestor of a new sequence  $k' \rightarrow k'/2$  and so on, presumably preserving DSI.

#### E. Signatures of the period-doubling cascade

Our purpose so far was mostly to point out that DSI was a worthwhile *hypothesis* in the needle growth model. We think there is enough evidence that it might be there to actually investigate the question numerically in some details. Let us now recall some standard results for the needles growth. Introduce  $n(y)$  the number density of needles extremities, such that  $n(y)dy$  is the total number of needles whose extremities are in  $[y, y+dy]$ . There is a number of theoretical arguments confirmed by numerical simulations that lead to the following asymptotic form [16,15]:

$$n(y) \propto y^{-2}, \quad y \rightarrow \infty,$$

where the limit  $y \rightarrow \infty$  is taken after the limit  $N \rightarrow \infty$ ,  $N$  the number of needles. The discrete scale invariance, if it is indeed generated by the dynamics, would lead to corrections of the form [4]

$$n(y) \propto y^{-2} [1 + A \cos(\omega \ln y + \phi)]$$

if the needles set was really a discrete regular fractal. However, even if DSI settles in, this can only occur with fluctuations. By analogy with the case of a random discrete fractal, where the rescaling factor fluctuates at every renormalization iteration [4], the previous formula should be replaced by

$$n(y) \propto y^{-2} [1 + Ay^{-\alpha} \cos(\omega \ln y + \phi)], \quad (2.23)$$

where  $\alpha$  depends on the fluctuations of the rescaling factor  $\lambda$ ,  $\omega = 2\pi/\ln \lambda$ , where  $\lambda$  is an ‘‘average’’ [4] of the rescaling factors. From the above discussion we expect  $\lambda \approx 2$ .

Now, a form similar to Eq. (2.23) has been recently found in DLA, with  $n(y)$  replaced by the mass density at distance  $r$  from the center of the cluster. Actually, a surprise of the studies in [5] is that *two* periods occur with comparable amplitudes in Eq. (2.23), corresponding to  $\lambda \approx 2$  and  $\lambda \approx 4$ . It is important to stress that the latter is not a sort of ‘‘harmonic’’ of the former. Indeed, in a discrete regular fractal, invariant under scale transformations with generator  $x \rightarrow \lambda x$ , the allowed values of  $\omega$  would be of the form  $n(2\pi/\ln \lambda)$  corresponding to successive roots  $\lambda^{1/n}$  of  $\lambda$ , not integer powers. Moreover, the successive harmonics would decay exponentially fast. The presence of the two terms in DLA was actually interpreted by saying that the discrete RG transformation appropriate for DLA, i.e., the one of which DLA is the invariant measure, is made of two portions of straight lines with respective slopes  $\lambda$  and  $\lambda^2$ , leading to a log-‘‘quasiperiodic’’ behavior [17]. This is quite far from the naive picture we proposed earlier, and surely there is a big theoretical gap to be filled in to explain this phenomenon. By simple analogy with DLA, having in mind that DSI is produced by the same mechanism in both problems and that DLA branching is irrelevant for that matter, we thus look more generally for an expression of the form [5,4]

$$n(y) \propto y^{-2} \left[ 1 + \sum_i A_i y^{-\alpha_i} \cos(\omega_i \ln y + \varphi_i) \right]. \quad (2.24)$$

A similar expression with an exponent  $-1$  would hold for the cumulative quantity  $N(y)$ , the number of needles of height greater or equal to  $y$ .

### III. NUMERICAL SIMULATIONS

#### A. The angle screening model

The most efficient way of simulating the Laplacian growth model is by using random walkers [18]. We release them from the top of the system and let them move at random until they approach the needles. If a mover touches the side of a needle, it then disappears and another one is generated. If the mover passes through the empty site immediately above the top of a needle it sticks to it, and the needle height increases by one unit. This model does not give spectacularly good results. The reason is presumably the presence of logarithmic corrections to scaling, as argued in [15]. In fact, even for very big systems, the exponent of  $n(y)$  is poorly reproduced. We will present results for this model later on.

To start, we will also use another model that is supposed to be in the same universality class, but probably has negligible logarithmic corrections. This model is the angle screen-

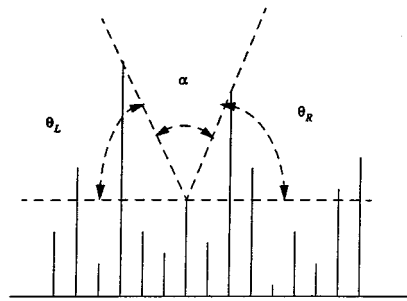


FIG. 4. Growth rules for the angle screening model.

ing model [19]. To simulate it, we start with an array of needles of random arbitrary heights. We then let each needle grow according to the following rule. For a given needle, look at the maximum left ( $\theta_L$ ) and right ( $\theta_R$ ) screening angle determined by all the other needles (Fig. 4). We define the ‘‘open view angle’’  $\alpha$  to be

$$\alpha = \pi - \theta_L - \theta_R, \quad (3.1)$$

the growth rate is then taken to be proportional to this angle  $\alpha$ , normalized by  $\pi$  up to some power  $\eta$  ( $\eta$  model),

$$v \propto \left( \frac{\alpha}{\pi} \right)^\eta, \quad (3.2)$$

so the highest needle has the greatest growth rate, i.e., increases by one unit each step, while shorter ones have a smaller growth rate. This is supposed to simulate the screening effect. Intuitively the chance for one needle to get some outside material necessary to its growth is proportional to the area enclosed in this open view angle  $\alpha$ . Periodic boundary conditions have been used in the computation of the growth rate at every step.

The results for the exponent of the second model are known to be much better and very close to the theoretical value. We have generated ten samples of  $N = 3000$  needles for  $\eta = 1$ . We have usually let this sample grow until the highest needle reaches the height  $N$ . In this case, the system having comparable  $x$  and  $y$  sizes can be expected to reproduce fairly well the asymptotic regime in which we expect a dependence like Eq. (2.24) to hold. For each sample, we have first considered the integrated quantity  $N(y)$ , the number of needles of length greater than or equal to  $y$ . At small and large  $y$ , it is expected to behave in a nonuniversal way. For small  $y$ , this is because the asymptotic behavior is expected to hold only for large  $y$ . For too large  $y$ , this is because  $N$  is finite, so the region is very badly sampled. On every sample, there is a region close enough to the asymptotic regime. This can be checked by plotting the logarithm of  $N(y)$  as a function of  $\ln y$  (we use here *decimal* logarithms) and finding the region where the plot is well approximated by a straight line (see Fig. 5 for an example). This region somewhat varies from sample to sample, but is always around  $y \in [150, 2700]$ . That we are close to the asymptotic regime is checked by the value of the exponent that fluctuates from sample to sample but is always found in the region  $m \in [0.96, 1.04]$  (the exponent is much better than in the Laplacian model, probably because the logarithmic corrections have a much smaller amplitude). For this

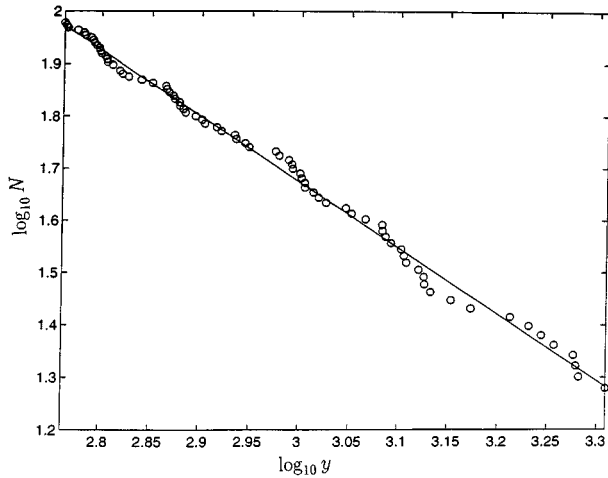


FIG. 5. A typical example of the cumulative distribution  $N(y)$  of needle lengths for the angle screening model, together with the best fit using a power law. The corresponding exponent is 1.0254, very close to the asymptotic value 1. Regular oscillations are clearly visible.

asymptotic region, one usually identifies oscillations around the straight line that can be fitted by formula (2.23) [we do not yet consider Eq. (2.24), which would involve too many fitting parameters here]. Several methods of fit are possible; in particular, one can fit  $N(y)$  or its logarithm. The latter case seems to reproduce more stable results. Out of ten samples, seven values of  $\omega = 2\pi/\ln \lambda$  ( $\ln$  is the decimal logarithm) are in the region  $\omega \in [8, 12]$  (corresponding to  $\lambda \in [3.3, 6.0]$ , with three values very close to  $\omega \approx 10.4 = 2\pi/\ln 4$  ( $\lambda \approx 4$ ), one value was about twice as big  $\omega \approx 21$  ( $\lambda \approx 2$ ), and two values were much lower, with  $\omega \leq 5$  ( $\lambda > 18$ ), and probably not significant. Indeed, several things have then to be noticed. First, the range of values of  $y$  defines an interval in logarithmic scale  $\Delta \ln y = \ln y_{\max}/y_{\min}$ , with a value  $\Delta \ln y = 1.2$ , corresponding to  $\omega = 5.0$ . Any value of  $\omega$  lower than this cutoff corresponds merely to fitting the finite sample size and cannot be considered significant, ruling out two samples. For the remaining significant values of  $\omega$ , the  $\chi^2$  is improved by a factor between 2 and 3. On a typical sample, as in Fig. 5, it is also clear that other frequencies are relevant, corresponding to roughly an  $\omega$  two times bigger.

At this stage, it is useful to stress that we are looking for a rather elusive quantity. The amplitude of the log-periodic term is expected to fluctuate from sample to sample [4, 5]. Moreover, the values of  $\omega$  are also expected to fluctuate from sample to sample, in a way that can be handled in simple models [4], but is largely unknown here. For comparison, we perform in the Appendix the same analysis for random numbers generated following a power-law distribution with the same exponent 1. In other words, we test the null hypothesis that the log-periodic oscillations could just be due to normal fluctuations in a power-law distribution. In the Appendix, we are able to reject this null hypothesis at an extremely high confidence level.

To get more precise information, we have constructed, like in the DLA case [5], the ‘‘local dimension.’’ This quantity is obtained by

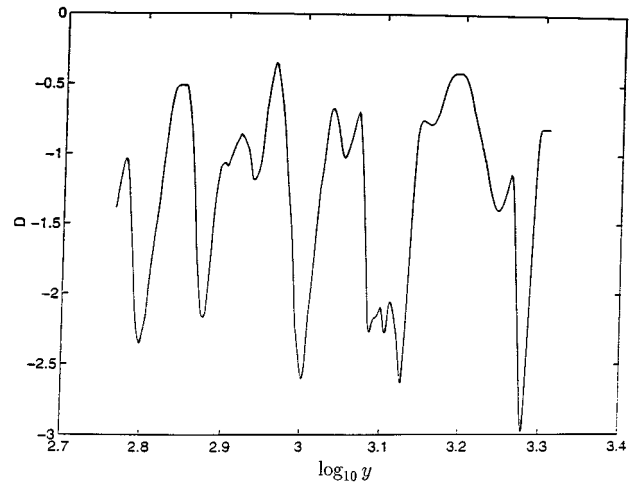


FIG. 6. The local dimension  $D(y)$  obtained as the local logarithmic derivative (3.3) of  $N(y)$  shown in Fig. 5. Note that the oscillations are much more visible.

$$D(y) = \frac{d \ln N}{d \ln y}, \quad (3.3)$$

and according to Eq. (2.24) it should go like

$$D(y) = -1 + \sum_i A_i y^{-\alpha_i} \cos(\omega_i \ln y + \phi_i). \quad (3.4)$$

The function  $D(y)$  for a typical sample is represented in Fig. 6, where regular oscillations are clearly visible. Since we expect the two main values of  $\omega$  to play comparable roles, rather than doing a fit of this form, it is much better to look at the Fourier spectrum (in variable  $\ln y$ ) of  $D(y)$ . This was done by a variety of techniques, in particular the Lomb periodogram, to get rid as much as possible of the effect of the damping term  $y^{-\alpha}$  in Eq. (3.4). As in [5], we represent the results of this study by considering histograms of the peaks of the Fourier spectrum. Since we do not have a large number of samples, we present the results in a manner most suitable to get rid of the noise. We thus only consider the two main peaks of the periodogram for each sample. From the set of these peaks, we construct their cumulative distribution, and then smooth it. Its derivative then provides the density probability to obtain a given frequency in Fourier space. The result is shown in Fig. 7. This histogram is defined on the interval  $\omega \in [\omega_{\min}, \omega_{\max}]$  where  $\omega_{\min} \approx 5$  ( $\lambda \approx 18$ ) is determined by the size of the sample, and  $\omega_{\max} \approx 35$  ( $\lambda \approx 1.5$ ) is determined by the typical distance between sample points. We observe three peaks in this histogram, corresponding, respectively, to values  $\lambda = 3.7 \pm 0.4$ ,  $\lambda = 1.9 \pm 0.2$ , and  $\lambda = 1.4 \pm 0.3$ . The peak at  $\lambda \approx 2$  is clearly significant, being well away from the small and large  $\omega$  cutoffs. The other two peaks are unfortunately quite close to our cutoffs, and it might be safer to discard them as nonsignificant. However, we observe that the first peak is close to the value  $\lambda \approx 4$  of the DLA case. Also, the third peak is close to  $\lambda = \sqrt{2}$ , and could well be interpreted as a harmonic.

Finally, as was observed in the DLA case [5], we have checked that the oscillations disappear when quantities such as  $N(y)$  are averaged over the ten samples—what remains is

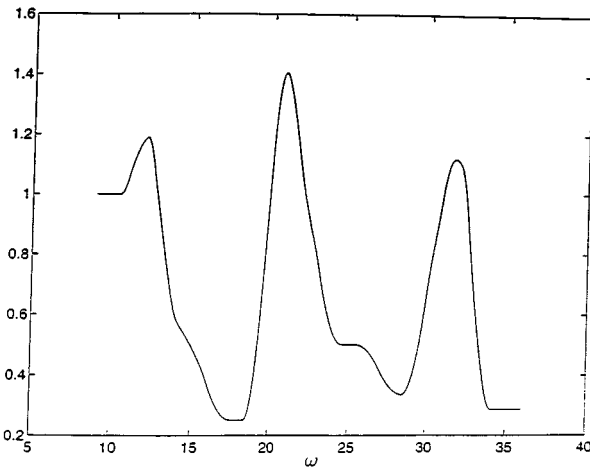


FIG. 7. The histogram of the two main peaks of Lomb periodograms performed on  $D(y)$  for ten samples.

simply noise decorating the simple power law. We think that this is due to random dephasing of the log-periodic oscillations due, in particular, to finite size effects as discussed in [4]. Since most authors considered only averages of  $N(y)$  to get a better statistics, they could not observe the log-periodic oscillations.

### B. $\eta$ model

We have performed a similar analysis in a variant of the model where the screening goes as a power of the screening angle. We present the results obtained for  $\eta = \frac{1}{2}$  ( $\eta = 1$  previously). For an unknown reason, the asymptotic region appears smaller in that case,  $y \in [700, 2800]$ . The exponent changes and we find a value  $\approx 1.25 \pm 0.15$  instead of 1 previously for  $\eta = 1$ . The same analysis was performed for  $D(\ln y)$ , leading to the histogram of frequencies shown in Fig. 8. We observe a slight shift towards higher frequencies but the pattern is totally consistent.

### C. Random-walker algorithm

For the original random diffusion model, the simulation takes a much longer time. Moreover, as commented above,

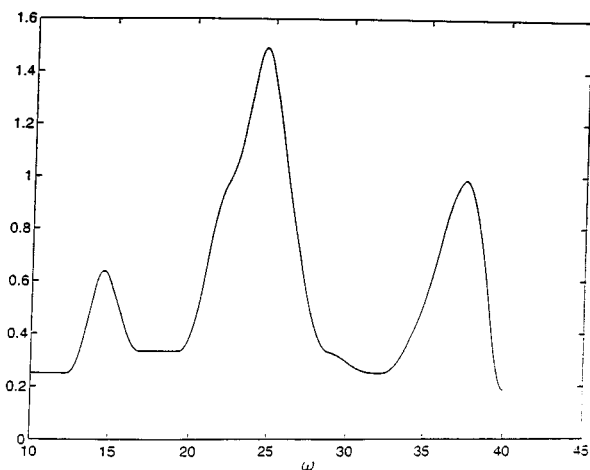


FIG. 8. The histogram of the two main peaks of Lomb periodograms performed on  $D(y)$  for the  $\eta$  model for  $\eta = 0.5$ .

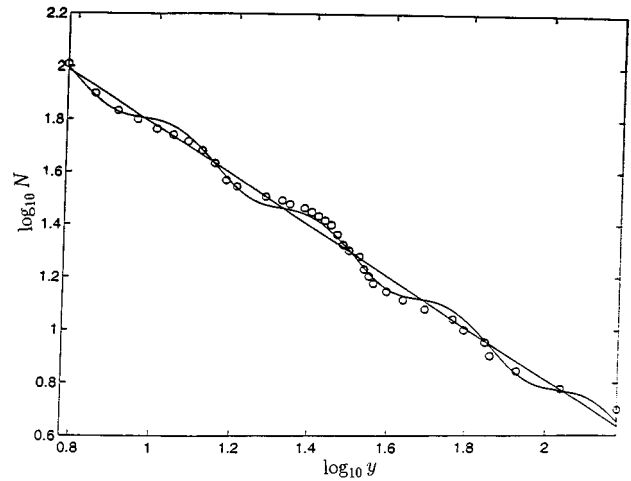


FIG. 9. A typical example of cumulative distribution  $N(y)$  for the random-walker algorithm.

one does not expect too good results anyway due to logarithmic corrections [15]. Figure 9 shows the cumulative distribution  $N(y)$  of a typical sample, and Fig. 10 the corresponding local dimension  $D(\ln y)$ . The log-periodic oscillations are nevertheless clearly visible, with  $\lambda \approx 2$ . We have not tried to get a strong statistics in this case as the DLA case has been treated extensively with very large statistics in [5] and the random-walker algorithm for the needle problem is bound to perform poorly compared to the angle screening model.

## IV. A MODEL OF CRACK GROWTH

The previous study deals with a rather idealized situation. As we expect the generation of discrete scale invariance to be universal in the same sense as critical exponents are, and to depend only on general properties, here instability and screening, it is useful to generalize our study to more realistic models that can be compared to experiments. We thus revisit the crack problem in which the cascade of period doubling was first envisioned for thermally induced cracks in brittle solids [6].

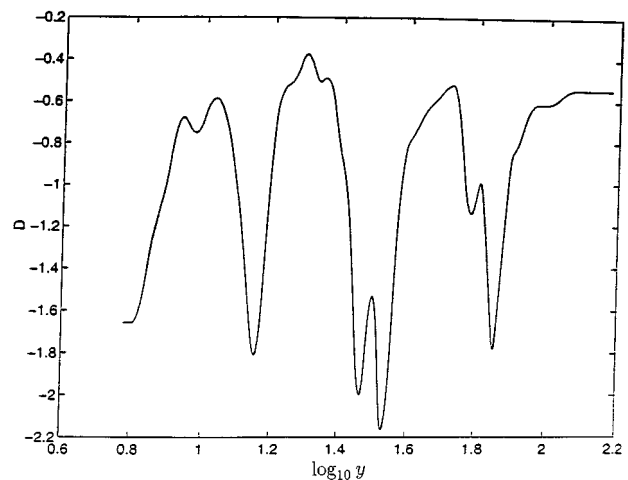


FIG. 10. The local dimension  $D(y)$  obtained as the local logarithmic derivative (3.3) of  $N(y)$  shown in Fig. 9.

### A. Single crack growth

Consider the problem of crack growth in antiplane stress. In the case of a remotely applied antiplane shear stress applied at infinity in a plane parallel to the  $(y, z)$  plane, both the displacement  $u_z$  and stress field  $\sigma_{xz}$  obey Laplace's equation: this situation is known as "antiplane" stress and reduces the tensorial elastic equation into a scalar problem [20]. In the presence of a crack of length  $2a_1$  parallel to the shear plane, the previously uniform stress field is modified so as to obey Laplace's equation with the boundary condition of vanishing stress on the crack edges [21]. As a consequence, the stress is reduced near the crack edges, but is enhanced at the crack tips and the growth occurs there. Ideally, there is a stress singularity at the cracks tips, which is the exact counterpart of the one found for the gradient of the field in the needle model. In the mechanical literature, the stress intensity at crack tips is described by the so-called *stress intensity factor*, noted as  $K$ . The growth of cracks is controlled by  $K$ . The stress intensity factor depends on the intensity of the remote applied stress, on the geometry of loading, and on the crack length. The intensity of stresses in the region near the crack tip is proportional to  $K$ . For the general case where the stress field  $\sigma(x, y)$  is nonuniform but symmetric  $\sigma(x, y) = \sigma(x, -y)$ , one has [22].

$$K = \frac{2}{\sqrt{\pi a_1}} \int_0^{a_1} \frac{\sigma(0, y)}{[1 - (y/a_1)^2]^{1/2}} dy, \quad (4.1)$$

which reduces to the well-known relationship  $K = \sigma \sqrt{\pi a_1}$  in the uniform case. Classical brittle fracture mechanics is based on the fact that as long as  $K$  has not reached a critical value  $K_c$ , the crack remains stable. If  $K$  becomes greater than  $K_c$ , the crack propagates, in general in an unstable manner, with a velocity equal to a fraction of the speed of sound, leading ultimately to the total breaking of the medium. However, a lot of experimental evidence that has been rationalized theoretically shows that a crack does not remain stable, even below  $K_c$  [23]. This is the so-called *slow crack growth* regime. This growth is thermally activated and depends on the chemical properties of the fluids that can fill the crack leading to corrosion-assisted crack growth. In this regime, which is the most often encountered practically, the crack tip velocity is found to be proportional to  $K^m$  with  $m$  ranging from 2 to 60 depending on the material and conditions. In the ideal limit of a dried vacuum, the thermal fluctuations prevail and theoretical analysis shows that, at sufficiently small stress  $\tau$ , the crack tip velocity is proportional to  $K$ . This is exactly the growth law (2.2) used for the needle problem studied above, since  $\lim_{r \rightarrow 0} \sqrt{r} |\nabla \phi(r + r_i)|$  is nothing but the (stress) intensity factor. The  $\eta$  model would then correspond to the more general situation  $m \neq 1$ .

### B. Crack interactions

Consider two parallel cracks with their centers along the  $x$  axis. The computation of the stress intensity factor of each crack in the presence of the other one is a difficult task. Each stress intensity factor is, in general, smaller than its value when isolated, exemplifying again the effect of screening. The larger of the two cracks will be less screened and will

thus grow faster, eventually stopping the smaller crack. We have discussed this phenomenon in Sec. II. Generalizing to many cracks, the mechanical literature uses finite or boundary element methods [24], or various approximation schemes [25]. Here, we investigate a system of thousands of cracks and thus need an efficient algorithm. This can only be obtained with some approximation, which we now explain.

The approximation we use is the pairwise "double-scattering" interaction scheme. Consider a crack of length  $a_1$  parallel to  $y$  at  $x=0$  in a medium where the stress field is originally uniform. Near this crack, the stress field becomes nonuniform, and we denote it by  $\sigma_1(x, y)$ . It is calculated exactly by conformal techniques. Introduce a second crack of length  $a_2$  at a distance  $X$  from the previous one. The pairwise double-scattering approximation consists in calculating the stress intensity factor of the second crack as

$$K_2 = \frac{2}{\sqrt{\pi a_2}} \int_0^{a_2} \frac{\sigma_1(X, y)}{[1 - (y/a_2)^2]^{1/2}} dy, \quad (4.2)$$

where  $\sigma_1(x, y)$  is the foregoing stress field in the medium due to crack 1 only. Similarly, the stress intensity factor of crack 1 is estimated by

$$K_1 = \frac{2}{\sqrt{\pi a_1}} \int_0^{a_1} \frac{\sigma_2(0, y)}{[1 - (y/a_1)^2]^{1/2}} dy, \quad (4.3)$$

where  $\sigma_2(x, y)$  is the stress field that would exist due to crack 2 only. Notice that the stress field is modified once by one crack, which is then applied to the other crack, hence the term "double scattering." We can summarize this approximation by writing

$$K_i = K_i^0 C_i^j,$$

where  $K_i^0$  is the stress intensity factor of crack  $i$  in the absence of crack  $j$ , for a homogeneous remotely applied stress  $\sigma$ .  $C_i^j$  is a correction factor that expresses the action (4.2) of crack  $j$  on crack  $i$ .

For  $N$  parallel cracks,  $k=1, \dots, N$ , we make an additional approximation that the stress intensity factor of a crack  $i$  can be written as a product of multiplicative corrections

$$K_i = K_i^0 \prod_{k=1}^N C_i^k,$$

each of the correction factors  $C_i$  being calculated using the pairwise double-scattering scheme. Note that, for small corrections  $C_i^k$  close to 1, this multiplicative scheme is the same as the alternative additive one, up to first order in  $C_i^k - 1$ . The additive scheme provides, in general, a lower bound and is unable by construction to account for cooperative effects. The present multiplicative scheme mimics the nonlinear cooperative behavior of multicrack assemblies.

At each time step, we calculate the stress intensity factor  $K_i$  of each crack  $i$  according to these equations and increase each crack length by an amount proportional to  $K_i$ . This amounts to using the  $m=1$  growth law.

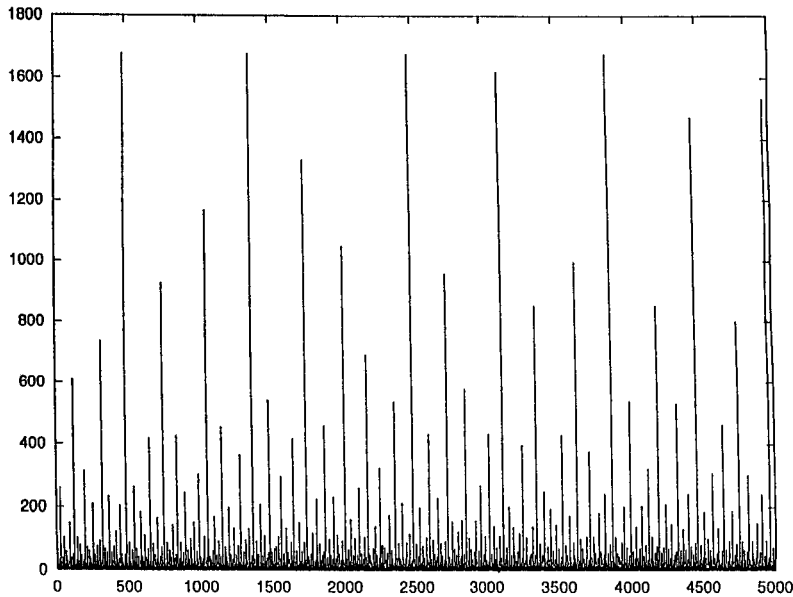


FIG. 11. Map of the 5000 cracks that have grown according to the rules described in the text. This configuration corresponds to the time where the largest crack has a length equal to one-third of the size of the system.

### C. Results of the growth of a population of cracks

Using the previously defined model, the log-periodic oscillations are strikingly more visible than for the previous simulations for the needle problem. This is probably due to the fact that our approximation scheme enhances the growth of large cracks in comparison to small cracks and thus both the instability and screening mechanisms.

We simulate 5000 cracks, of initial length randomly chosen between 0.49 and 0.51. The spacing between two cracks is also chosen randomly in the interval  $[0.99; 1.01]$ . Periodic boundary conditions are introduced along  $Ox$ . The computation stops when the largest crack reaches a length equal to one-third of the size of the system, corresponding to a length approximately equal to 1666. The density distribution of crack lengths is then computed using a logarithmic binning introduced in [3], which is optimized for power-law distributions. Figure 11 shows the 5000 cracks that have grown.

Notice that one can almost see with the bare eye the preferred scale ratio 2 in the crack lengths. Figure 12 shows the density distribution of crack lengths obtained for a typical simulation. A power-law behavior is found over more than three decades, with an exponent again equal to 2, in agreement with the law  $n(y) \propto y^{-2}$  found for needles [16,15]. Indeed, since we use here antiplane elasticity, the problem is scalar and is in the same universality class as the initial needle problem. Figure 13 presents the difference between the data and the linear trend (in log-log plot, qualifying the power law). Very clear oscillations can be observed. Figure 14, shows the Lomb periodogram, which suggests the existence of a single peak at  $\lambda = 2$  precisely. We performed six realizations of these simulations and observed that the exponent is very close to 2 ( $1.99 \pm 0.01$ ). The dispersion in the discrete scaling ratio  $\lambda$  is found to be larger:  $\lambda = 2.25 \pm 0.3$ .

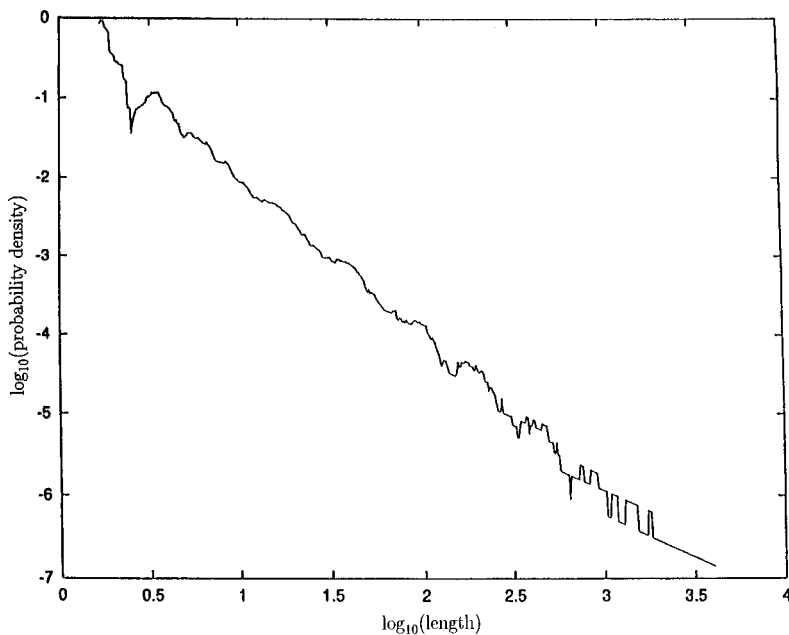


FIG. 12. Density distribution of crack lengths obtained for a typical simulation.

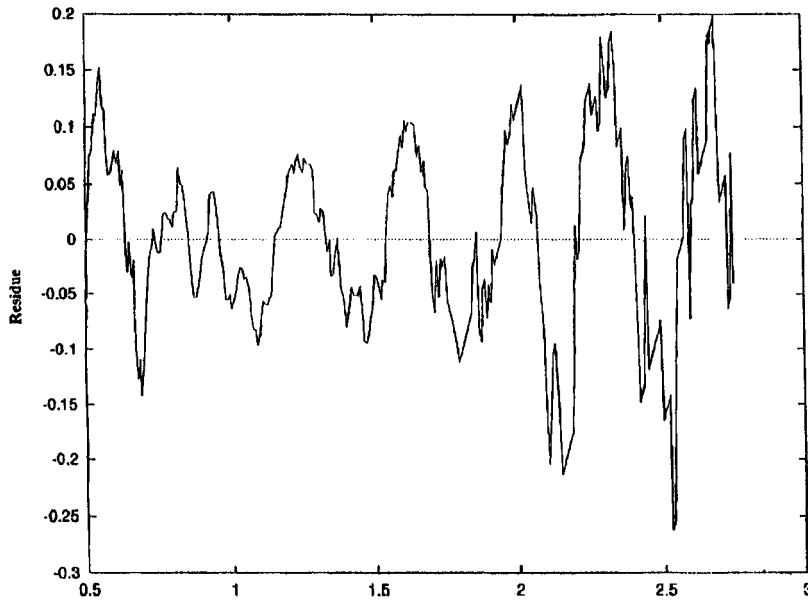


FIG. 13. Difference between the density distribution and the simple power-law behavior (linear in log-log plot), showing the (log-periodic) oscillations.

#### D. Real geological cracks

In addition to the evidence presented in [3], we present other data found for cracks in rocks (also called joints in the geological literature) in Fig. 15. In Fig. 15(a), the joints are presumably formed under thermal stressing upon cooling of volcanic rocks in Hawaii. We can see with the bare eye evidence of size ratios 1:2:4 approximately. This situation is probably close to the one analyzed in [6]. The other data set shown in Fig. 15(b) has been sampled at a road cut near Watkins Glen at the southern tip of Seneca Lake, New York. We do not know the stressing conditions, only that the joints correspond mainly to mode I cracks working in the opening tensile mode. Figure 16 shows the Lomb periodogram of the data set of Fig. 15(b) [15(a) contains too few cracks], showing good evidence of discrete scale invariance with a preferred scaling ratio close to 2. The realization that screening is important for crack propagation in basalt has been dis-

cussed in [26]. The mechanism whereby cracks grow and are selected, with only a few finally “surviving” at lengths as large as in Fig. 11 has also been noted for joints [27]. However, the period-doubling mechanism studied in the present paper has not been pointed out. It is also noteworthy that the screening and instabilities, the two key ingredients for the appearance of the period doubling, are as effective in the scalar (needle) problem as in the tensorial (crack) case.

#### V. CONCLUSION

Motivated by evidence of discrete scale invariance, in the form of log-periodic oscillations, from simulations on diffusion limited aggregation [5] and from crack data [3], we have performed an analysis of a simplified model of DLA, the needle problem, which has also direct application to crack growth. Based on perturbative analysis and some exact re-

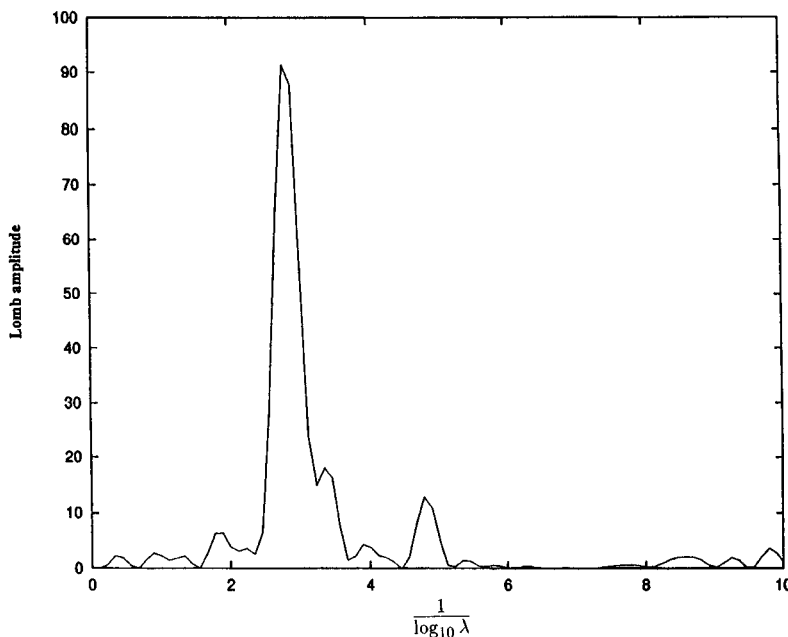


FIG. 14. Lomb periodogram of the data presented in Fig. 13 showing a well-defined peak at  $\lambda \approx 2$ .

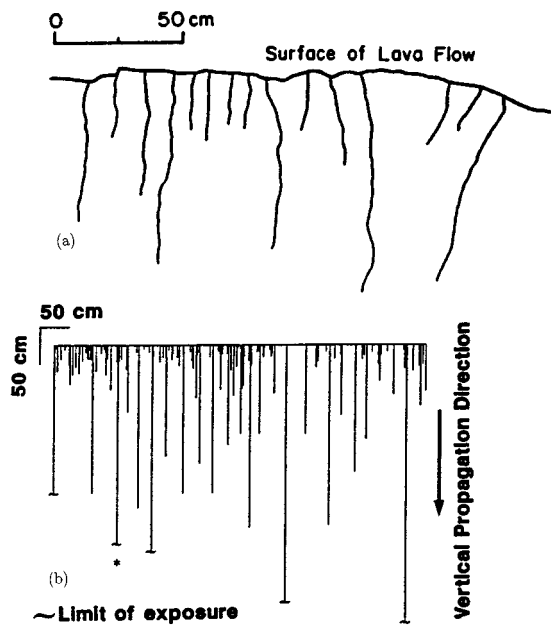


FIG. 15. (a) Joints in volcanic rocks from thermal stressing, Volcano National Park, Hawaii; (b) a road cut near Watkins Glen at the southern tip of Seneca Lake, New York, showing joints in Silfstone and shales.

sults from the hodograph method, we have suggested that the two basic ingredients leading to DSI are the short-wavelength Mullins-Sekerka instability and the strong screening of competing needles. These analytical results have been supplemented by numerical simulations for the needle problem, using various growth rules (DLA, angle screening,  $\eta$  model, crack approximation) on systems containing up to 5000 needles. The density of needles as a function of the distance to the base presents clear evidence of log-periodic modulations of the leading algebraic decay. We have also presented a comparison with geological data on joints exhibiting approximately the log-periodic structure. What we learn by comparing these different systems, with various growth rules, is that the spontaneous formation of

DSI seems robust with respect to significant modifications, giving confidence in its relevance.

The basic simple picture that emerges is that *nonlinear* interactions between the unstable modes of the set of needles lead to a succession of period doubling, the next subharmonic catching up, and eventually screening of the leading unstable mode. The succession of these period doublings, similar to an inverse Kolmogorov cascade, explains the existence of discrete scale invariance in these systems. We thus think that short-wavelength instabilities of the Mullins-Sekerka type supplemented by a strong screening effect provide a general scenario for the *spontaneous* formation of log-periodic structures. This scenario provides, in addition, an explanation of the ubiquitous observation of a preferred scaling ratio close to 2.

One might wonder to what extent having a discrete periodic structure at the beginning is essential to generate discrete scaling. Small fluctuations around this periodic structure do not seem to spoil DSI. This was clear in the simulations of Sec. IV, where the intervals between cracks were taken to fluctuate in the interval  $[0.99, 1.01]$ . We also checked in the angle screening model of Sec. III that the results were similar when we started with an array of cracks of random original lengths, which, due to screening, should be equivalent to having fluctuating crack intervals. For very large fluctuations of crack intervals, it is possible that DSI might disappear. Let us observe, however, that all the known mechanisms leading to extensional cracking produce a regular periodic array of nucleating cracks. For instance, in elastic flexure the period of the regular crack array is exactly given by the characteristic flexural length determined by the plate thickness and the elastic constants [28]. This is also true for elastic-plastic flexure and buckling [29], viscous necking [30], for instabilities in viscous or plastic layers [31], and for the shear lag mechanism used by material scientists [32] to explain morphologically similar patterns of regularly spaced tensile cracks on the brittle surface of layered composites, which has recently been proposed to explain the small-scale fracture patterns on the volcanic plains of Venus [33].

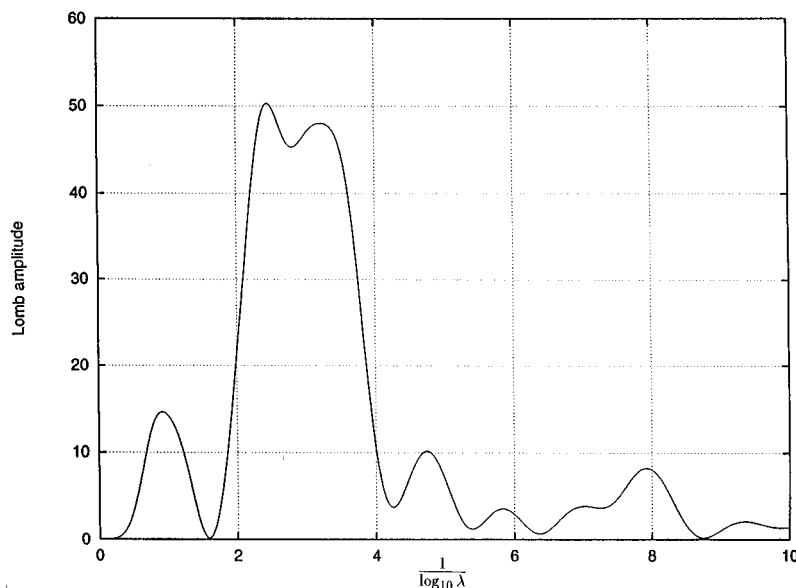


FIG. 16. Lomb periodogram of the data presented in Fig. 15(b) showing a well-defined peak at  $\lambda \approx 2$ .

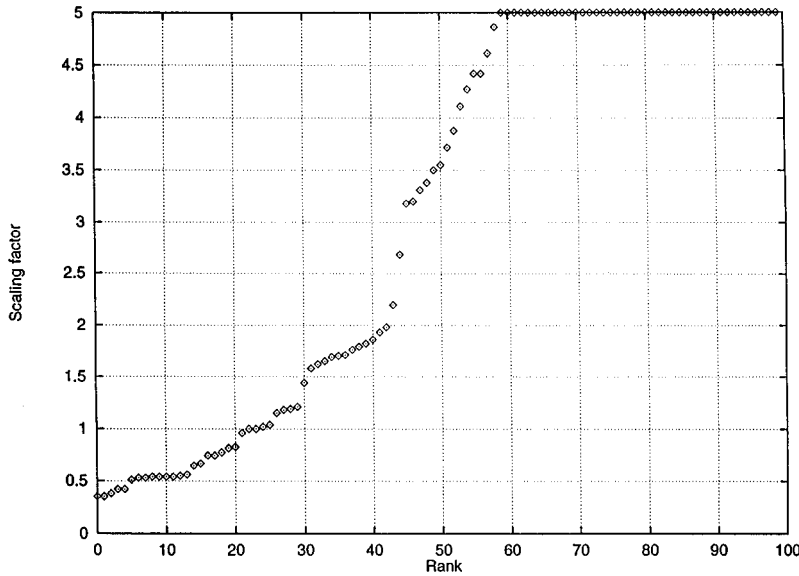


FIG. 17. The histogram of values of  $\lambda$  obtained by fitting the synthetic samples constructed from the Lévy law (A1) to a form like Eq. (2.24).

For growth models, the initial discreteness stems from the finiteness of the aggregating particle. In the case of DLA on a lattice, the discrete mesh creates the initial small-scale periodicity. For off-lattice DLA, we still have the intrinsic size of the particles. In the cylindrical geometry, which can be directly compared to our simulations on the needles, this implies that trees are at least separated by one particle diameter, leading again to an ultraviolet cutoff and approximate periodic structure.

To conclude, let us mention tentative connections with other works. In [34], it was shown that growth processes possess generally periodic and quasiperiodic *linear* oscillations in time and space, stemming from a beating of two length scales, here the distance between the needles and the penetration depth. In a fractal, since the relevant length scales change as the structure grows in a self-similar fashion, could this transform the periodic or quasiperiodic beating into a log-periodic one? It would also be interesting to understand how the DSI can be accounted for by the theory of DLA developed in [35]. Finally, Carleson and Makarov have obtained some rigorous results concerning the needle model [36] that seem to confirm the period-doubling scenario.

#### ACKNOWLEDGMENTS

Y.H., G.O., and H.S. were supported by the DOE, the NSF (through the National Young Investigator program), and the Packard Foundation. We are grateful to J. V. Andersen, V. Hakim, J. Rudnick, and C. G. Sammis for very stimulating discussions at the early stages of this work. We especially thank C. Sammis for pointing out Ref. [6] to us, and J. Rudnick for mentioning Ref. [17] to us. We thank Professor A. Aydin for kindly providing the data on joints used to prepare Figs. 15 and 16. We also acknowledge exchanges with L. Carleson, T. Halsey, and R. Savit.

#### APPENDIX: COMPARISON WITH RANDOM SYNTHETIC DATA GENERATED WITH A PURE POWER-LAW DISTRIBUTION

In order to assess the significance of our analysis of the numerical and experimental data sets, we test it on a well-

controlled system. This is done in order to test the null hypothesis that our results could be the results of chance. We consider random numbers generated with a power law with density

$$n(y) \propto y^{-m-1}, \quad m=0.5. \quad (\text{A1})$$

We chose a value  $m=0.5$  instead of  $m=1.0$ , as the fluctuations are larger in the former case and spurious log-periodic oscillations might be easier to pick up. This choice,  $m=0.5$ , also applies to the data on geological joints analyzed previously [3]. We generate 100 sets of 600 such random numbers, all in the interval  $y=1-130$ , corresponding to the natural cutoffs in natural observations [3]. For each sample  $i$ , we construct the density distribution  $P_i(y)$  of the 600 values of  $y$ . Each histogram  $P_i$  is fitted with a power law, including the log-periodic corrections, using a simulated annealing procedure. The values of  $\lambda$  thus found are shown in Fig. 17. Figure 18 shows the statistics of  $\chi^2$  improvements obtained by using the log-periodic corrections. This should be compared with the factor of 2–3 of improvements found for the needles. The histogram of  $\lambda$  values is shown in Fig. 19. It has a cutoff at large wavelengths due to the finite size of the sample. It is noteworthy that no well-defined peak singles out any frequency. Of course, some samples exhibit log periodicities with  $\lambda$  close to 2. However, this value is not the most probable one. Longer wavelengths (smaller frequencies) are observed more often. Quantitatively, the histogram of Fig. 19 provides a likelihood function weighting the probability of observing a given (log) frequency as a result of chance. The random case thus differs very significantly from the results of our simulations and the crack data.

We also carried out Lomb periodogram analysis of the samples, with similar results. We find that approximately one out of three samples presents significant log-periodic structures, as qualified by the Lomb periodogram. In these samples with log-periodic structure, approximately one out of three shows an improvement of the  $\chi^2$  by a factor of at least 2 when using the log-periodic formula compared to the simple power-law fit. We thus infer that the probability of observing from pure chance, in a *single* sample, a log-

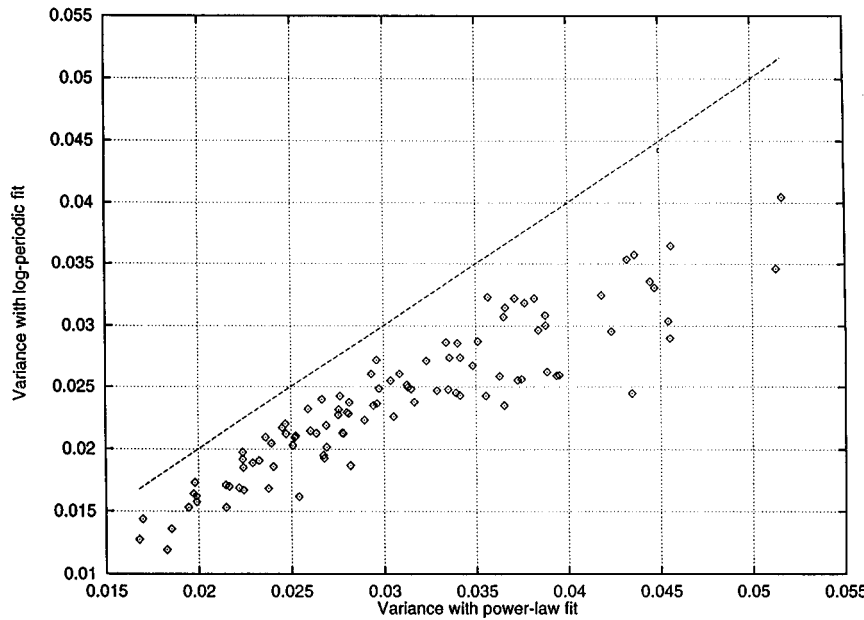


FIG. 18. The statistics of  $\chi^2$  improvements obtained by using a power law with log-periodic corrections compared with a pure power law.

periodic structure with quality comparable to our finding for the needles is about  $\frac{1}{9}$ . The probability of getting by pure chance log-periodic structures with quality comparable to our findings for the needles for seven samples out of ten (the results for our simulations on the angle screening model of needles) is thus  $P_{\text{nonLP}} = \binom{10}{7} (\frac{1}{9})^7 (1 - \frac{1}{9})^3 \approx 1.8 \times 10^{-5}$ . This extremely small number taken at face value would imply that our results are extremely significant statistically. However, we must take into account another source of error, namely, that, if the log-periodicity is genuine, the rate of success for its observation is not 100%, due to noise and statistical fluctuations. Indeed, in our ten needle simulations, we only observe well-defined log-periodic structures in seven out of ten samples. We thus ask, what is the probability of observing seven successes and three failures, *assuming* that the log-periodicity is genuine. We have only ten samples and the best we can do is estimate that the probability of not observ-

ing log periodicity when it should be there is  $\frac{3}{10}$ , our rate of success for the needles. Thus, the probability of observing three failures out of ten samples, *assuming* the systems must be log periodic is  $P_{\text{LP}} = \binom{10}{3} (\frac{7}{10})^7 (\frac{3}{10})^3 \approx 0.27$ . This is still much larger than  $P_{\text{nonLP}}$ .

To assess the statistical significance of our results, the standard statistical method is to use Bayes's theorem [37], which allows us to quantify precisely how our belief is modified by an observation or measurement. Suppose that  $p$  quantifies our initial belief in the existence of the log-periodic structure in the needles: in other words,  $p$  is the *a priori* probability for the log-periodic structure's existing as a *genuine* physical phenomenon. The simplest natural unbiased choice would be  $p = \frac{1}{2}$ , one-half probability of being genuine, one-half probability of not being there. If the reader is skeptical, he can choose a small value for  $p$ , say  $p_{\text{skeptics}} = 10^{-3}$ . Now, the question is: How do the measurements

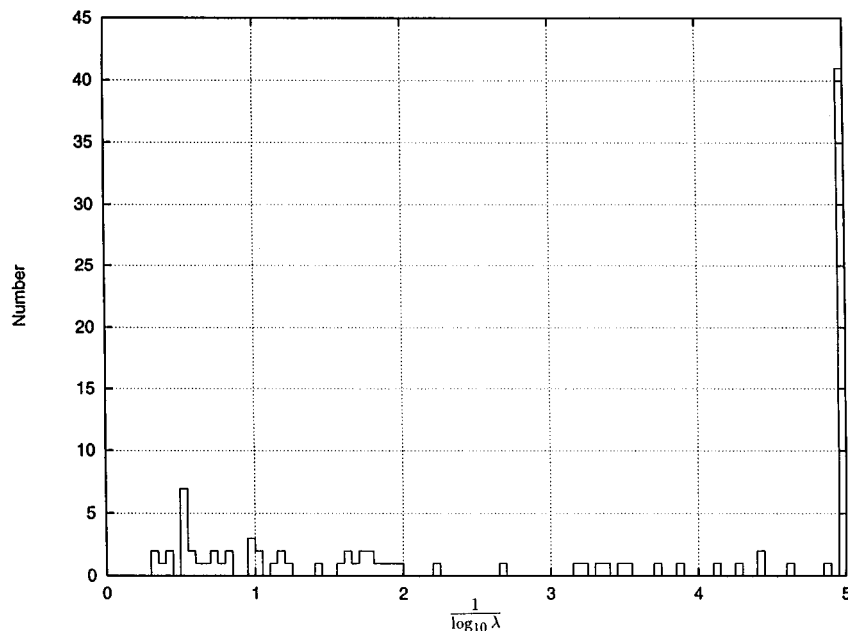


FIG. 19. The histogram of the most significant peaks of the Lomb periodogram of the local dimension in the synthetic Lévy sample.

we have made modify this *a priori* probability? Bayes's theorem states that the *a posteriori* probability  $p_{\text{post}}$  for the log periodicity's being genuine is proportional to the prior probability  $p$  times the likelihood. Quantitatively,

$$p_{\text{post}} = \frac{pP_{\text{LP}}}{pP_{\text{LP}} + (1-p)P_{\text{non LP}}}.$$

Plugging in the previous numbers, we find that this formula can be approximated by

$$p_{\text{post}} \approx 1 - \frac{1-p}{p} \frac{P_{\text{non LP}}}{P_{\text{LP}}}.$$

for  $p$  not too small. For instance, with  $p = \frac{1}{2}$ ,  $p_{\text{post}} \approx (1 - 6.7) \times 10^{-5}$ , i.e., a confidence level better than 99.99%. For skeptics, take  $p = p_{\text{skeptics}} = 10^{-3}$ . This yields  $p_{\text{post}} \approx 93\%$ , which is still quite statistically significant.

Of course, Bayes's theorem teaches us that it is impossible to convince someone diametrically opposed to a hypothesis (corresponding here to take  $p < 10^{-5}$ ). However, starting from a reasonable hypothesis ( $p$  not too small), the evidence we have presented strongly strengthens the case for the genuine existence of spontaneously generated log-periodic structures.

- 
- [1] J.-C. Anifrani, C. Le Floc'h, D. Sornette, and B. Souillard, *J. Phys. (France) I*, **5**, 631 (1995).
- [2] D. Sornette and C. G. Sammis, *J. Phys. (France) I*, **5**, 607 (1995); H. Saleur, C. G. Sammis, and D. Sornette, *Nonlinear Processes Geophys.*, **3**, 102 (1996); D. J. Varnes and C. G. Bufe, *Geophys. J. Int.*, **124**, 149 (1996); H. Saleur, C. G. Sammis, and D. Sornette, *J. Geophys. Res.*, **101**, 17 661 (1996); A. Johansen, D. Sornette, H. Wakita, U. Tsunogai, W. I. Newman, and H. Saleur, *J. Phys. (France) I* (to be published).
- [3] G. Ouillon, D. Sornette, A. Genter, and C. Castaing, *J. Phys. (France) I*, **6**, 1127 (1996).
- [4] H. Saleur and D. Sornette, *J. Phys. (France) I*, **6**, 327 (1996).
- [5] D. Sornette, A. Johansen, A. Arnéodo, J.-F. Muzy, and H. Saleur, *Phys. Rev. Lett.*, **76**, 251 (1996).
- [6] S. Nemat-Nasser, L. M. Keer, and K. S. Parihar, *Int. J. Solids Struc.*, **14**, 409 (1978); S. Nemat-Nasser and A. Oranratnachai, *Trans. ASME*, **101**, 34 (1979).
- [7] W. W. Mullins and R. F. Sekerka, *J. Appl. Phys.*, **3**, 444 (1964).
- [8] D. Bensimon, L. P. Kadanoff, S. Liang, B. Shraiman, and C. Tang, *Rev. Mod. Phys.*, **58**, 977 (1986).
- [9] J. Szép and U. Lugosi, *J. Phys. A*, **19**, L1109 (1986).
- [10] B. Derrida and V. Hakim, *Phys. Rev. A*, **45**, 8759 (1992).
- [11] A. Cebers and W. L. Luo, *J. Intell. Mater. Syst. Struct.*, **6**, 854 (1995); (private communication).
- [12] W. Losert, B. Q. Shi, H. Z. Cummins, and J. A. Warren, *Phys. Rev. Lett.*, **77**, 889 (1996).
- [13] J. A. Warren and J. S. Langer, *Phys. Rev. A*, **42**, 3518 (1990); *Phys. Rev. E*, **47**, 2702 (1993).
- [14] V. Hakim (unpublished).
- [15] J. Krug, K. Kassner, P. Meakin, and F. Family, *Europhys. Lett.*, **24**, 527 (1993).
- [16] M. Adda Bedia, Ph.D. thesis, Paris VI University, 1994 (unpublished).
- [17] A. Arneodo, F. Argoul, E. Bacry, and J. F. Muzy, *Phys. Rev. Lett.*, **68**, 3456 (1992); A. Arneodo, F. Argoul, J. F. Muzy, and M. Tabard, *Phys. Lett. A*, **171**, 31 (1992); A. Arneodo, F. Argoul, J. F. Muzy, M. Tabard, and E. Bacry, *Fractals*, **1**, 629 (1993).
- [18] P. Meakin, *Phys. Rev. A*, **33**, 1984 (1986); G. Rossi, *ibid.*, **34**, 3543 (1986); **35**, 2246 (1987).
- [19] R. Karunasiri, R. Bruinsma, and J. Rudnick, *Phys. Rev. Lett.*, **62**, 788 (1989); J. Krug, K. Kassner, P. Meakin, and F. Family, *Europhys. Lett.*, **24**, 527 (1993).
- [20] K. Aki and P. G. Richards, *Quantitative Seismology: Theory and Methods* (Freeman, San Francisco, 1980).
- [21] D. D. Pollard and P. Segall, in *Fracture Mechanics of Rock* edited by B. K. Atkinson (Academic, New York, 1987).
- [22] B. R. Lawn, *Fracture of Brittle Solids* (Cambridge University Press, Cambridge, England, 1993).
- [23] B. K. Atkinson and P. Meredith, in *Fracture Mechanics of Rock* (Ref. [21]).
- [24] J. E. Akin, *Finite Elements for Analysis and Design* (Academic, London, 1994); A. Portela, *Dual Boundary Element Analysis of Crack Growth* (Computational Mechanics Publications, London, 1993).
- [25] M. Kachanov and J. P. Laures, *Int. J. Fract.*, **41**, 289 (1989).
- [26] J. M. DeGraff and A. Aydin, *J. Geophys. Res.*, **98**, 6411 (1993).
- [27] D. D. Pollard and A. Aydin, *Geol. Soc. Am. Bull.*, **100**, 1181 (1988).
- [28] D. L. Turcotte and G. Schubert, *Geodynamics: Applications of Continuum Physics to Geological Problems* (Wiley, New York, 1982).
- [29] W. B. Banerdt and M. P. Golombek, *J. Geophys. Res.*, **93**, 4759 (1988).
- [30] S. C. Solomon and J. W. Head, *J. Geophys. Res.*, **89**, 6885 (1984).
- [31] M. T. Zuber, *J. Geophys. Res. Suppl.*, **92**, E541 (1987).
- [32] M. S. Hu and A. G. Evans, *Acta Metall.*, **37**, 917 (1989).
- [33] W. B. Banerdt and C. G. Sammis, *J. Geophys. Res.*, **97**, 16 149 (1988).
- [34] Z. Cheng and R. Savit, *J. Phys. A*, **19**, L973 (1986); R. Baiod, Z. Cheng, and R. Savit, *Phys. Rev. B*, **34**, 7764 (1986); Z. Cheng, R. Baiod, and R. Savit, *Phys. Rev. A*, **35**, 3134 (1987); R. Savit and R. K. P. Zia, *J. Phys. A*, **20**, L987 (1987); Z. Cheng, L. Jacobs, D. Kessler, and R. Savit, *ibid.*, **20**, L1095 (1987).
- [35] T. Halsey and M. Leibig, *Phys. Rev. A*, **46**, 7793 (1992); T. Halsey, *Phys. Rev. Lett.*, **72**, 1228 (1994).
- [36] L. Carleson and N. Makarov (unpublished).
- [37] J. A. Hartigan, *Bayes Theory* (Springer-Verlag, New York, 1983); J. S. Maritz and T. Lwin, *Empirical Bayes Methods with Applications* (Chapman and Hall, London, 1989).